Characteristics of a Large Diameter Radio-Frequency Negative Hydrogen Ion Source*)

Yuko SASAKI, Sho TAKAYAMA, Haruhisa NAKANO[1)], Atsushi KOMURO, Kazunori TAKAHASHI and Akira ANDO

Department of Electrical Engineering, Tohoku University, 6-6-05 Aoba-yama, Sendai, Miyagi 980-8579, Japan
[1)]*National Institute for Fusion Science, 322-6 Oroshi, Toki, Gifu 509-5292, Japan*

(Received 30 November 2015 / Accepted 7 April 2016)

The characteristics of a 230-mm-diameter radio-frequency (rf) negative hydrogen ion source are investigated by the measurements of electron density and temperature. A hydrogen plasma is produced by an inductively coupled discharge operated with an rf frequency of 300 kHz and a power of a few tens of kW, where a field-effect-transistor-based inverter power supply is used as an rf generator. The ion source has a magnetic filter for reduction of the electron temperature near the plasma grid used for the extraction of a negative ion beam. A high electron density greater than 10^{18} m^{-3} is successfully obtained for an operating gas pressure of 0.3 Pa. The electron temperature near the plasma grid is observed to decrease to about 1 eV with increasing magnetic field strength of the magnetic filter.

Keywords: RF ion source, NBI, ion source, negative hydrogen ion, FET-based inverter rf power supply

DOI: 10.1585/pfr.11.2405088

1. Introduction

Plasma heating is one of the key issues to realize a thermonuclear magnetically confined fusion reactor. Some heating techniques, such as ion cyclotron resonance [1], electron cyclotron resonance [2], and neutral beam injection (NBI) [3], have been investigated for decades, and their performances have been well improved. NBI is categorized into two types, i.e., negative and positive NBIs (N-NBI/P-NBI), where the negative/positive ion beams have to be neutralized to heat the fusion plasma core surrounded by a very strong magnetic field, i.e., the ion beam energy has to be transferred to that of neutral particles before the beam injection. When operating the NBI with the beam energy close to 1 MeV for International Thermonuclear Experimental Reactor (ITER), an N-NBI system is considered to be more efficient than a P-NBI system because the neutralization efficiency of negative ions is much higher than that of positive ions [4]. Therefore, developing the negative ion source is inevitable to develop the high-performance 1-MeV class NBI. Hydrogen negative ion sources with a beam energy above 100 keV have been developed and tested in fusion experiments [5, 6]. A long-pulsed N-NBI is required to produce the beam energy of ~ 1 MeV and beam current of ~ 200 A/m^2 for ITER.

There are two processes of negative ion production, called volume and surface production processes [7]. In the volume production process, hydrogen molecules are vibrationally excited by collisions with high energy electrons. The negative hydrogen ions are produced via a dissociative attachment process with low energy electrons. To increase the dissociative attachment process and to avoid the destruction of negative ions, it is necessary to decrease the electron temperature to less than 1 eV [7]. In the surface production, hydrogen ions or atoms capture electrons on the metal surface having a low work function. In order to enhance the production rate, a Cs vaporing method has been utilized [8–10]. To date, the approach of seeding Cs atoms to a plasma grid (PG: first grid in the extraction grid system) and heating the grid temperature up to 200 °C, has enabled the negative ion production rate. The low electron temperature less than 1 eV is still required near the grid because the energetic electrons easily destroy the negative ions. Comparing the two methods of the volume and surface processes, the latter has shown a better performance [9, 10].

The development of a radio frequency (rf) negative ion source is required for stable and long-pulsed operation because of its filament-free structures, one of the important issue is a development of a high density rf hydrogen plasma source [11–14]. Fantz *et al.* reported operation of a source in an inductively coupled mode with an rf frequency of 1 MHz and power < 150 kW [14]. One of the authors has proposed and demonstrated the high density plasma production in a small diameter (70 mm) source tube by applying a field-effect-transistor (FET)-based inverter power supply (~ 300 kHz), which can yield a high conversion efficiency of about 90% from dc to rf. As fusion reactors, including ITER requires a large-diameter ion beam source,

author's e-mail: yukosasaki@ecei.tohoku.ac.jp

*) This article is based on the presentation at the 25th International Toki Conference (ITC25).

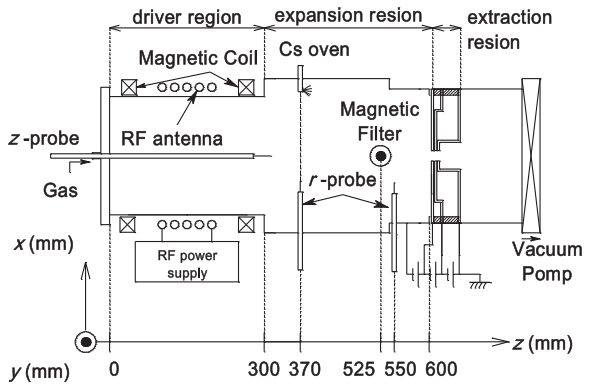

Fig. 1 Schematic of the large RF negative ion source.

the development of the large diameter, inverter-based, hydrogen negative ion source is one of challenging issues to be progressed.

Here, the source diameter of the rf negative ion source using the inverter rf power supply is enlarged up to 230 mm, which is almost the same diameter as that of the ITER NBI ion source. The basic characteristics of the plasma production and expansion are investigated with two different configurations of the magnetic filter.

2. Experimental Setup

A Schematic of the experimental setup is shown in Fig. 1, where the origin of z-axis is the surface of the upstream flange and the plasma grid (PG) is located at z = 610 mm. The negative ion source comprises a driver and expansion regions, as shown in Fig. 1. The driver region (an rf plasma source) comprises a 230-mm inner diameter and 300-mm-long ceramic tube with a 10-turn rf loop antenna wounded around the tube and surrounded by two magnetic coils. In the present study, the magnetic coils are not used. An exit of the driver region is connected to an expansion chamber (labeled expansion region in Fig. 1), and hydrogen gas is continuously introduced from the upstream flange via a mass flow controller. The previously described FET-based inverter rf power supply is used with the frequency of 290 kHz, where rf power is transferred to the rf antenna via an rf transformer and a LC resonance circuit [15]. Cs vapor is introduced from an oven located at z = 370 mm. A Line cusp magnetic field is produced using permanent magnets that are mounted on the upstream flange and expansion chamber to inhibit the energy loss to the wall.

Three cylindrical Langmuir probes with 0.9-mm-diameter tungsten tips are inserted from the upstream flange (labeled z-probe), and from the side ports of the expansion chamber at z = 370 and 550 mm (labeled r-probes). I–V characteristics of the Langmuir probes are analyzed with the assumption of a Maxwellian electron energy distribution.

The expansion region is a rectangular stainless steel vacuum chamber of 300 mm in width, 400 mm in height and 300 mm in length. Neodymium permanent magnets providing a magnetic filter are located at the downstream region of the expansion chamber, where two different configurations of the magnetic filter are tested. Figure 2 shows the axial profiles of the transverse magnetic field strength for filter configurations A (crosses) and B (open squares). These configurations are achieved by setting different numbers of the magnet pieces located at z = 540 and 525 mm for the configurations A and B, respectively. The maximum magnetic field strengths are 1.7 mT and 4.5 mT for the configuration A and B, respectively.

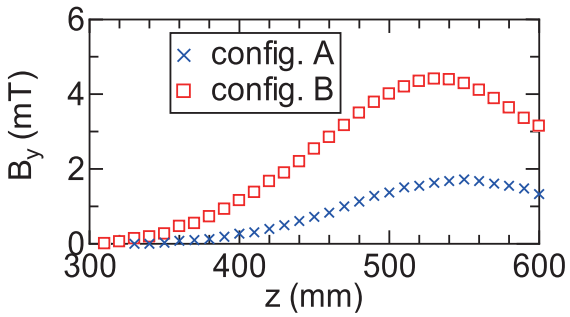

Fig. 2 Axial profiles of the magnetic filter field strength B_y for configuration A (crosses) and B (open circles).

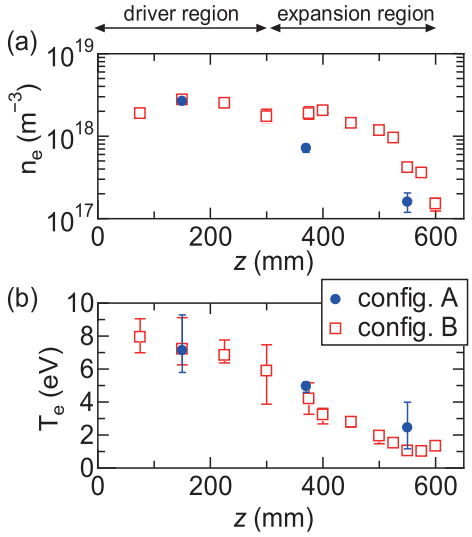

Fig. 3 Axial profiles of (a) the electron density and (b) the electron temperature for the pressure of 0.3 Pa, rf frequency of ~290 kHz, and P_{rf} ~ 18 kW. The data for configurations A and B are plotted using filled circles and open squares, respectively.

3. Experimental Results

Figure 3 shows axial profiles of the electron density (n_e) and electron temperature (T_e) measured by the z-probe for the operating pressure of 0.3 Pa, the rf power of P_{rf} = 18 kW, and the bias voltage of V_{bias} = 0 V, which

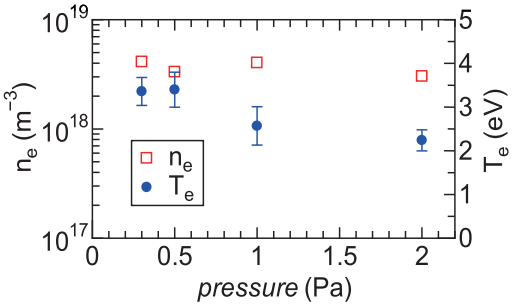

Fig. 4 The electron density (open squares) and the electron temperature (filled circles) as a function of the pressure measured at z = 370 mm, for the rf frequency of ~290 kHz, P_{rf} ~ 18 kW, and filter field configuration B.

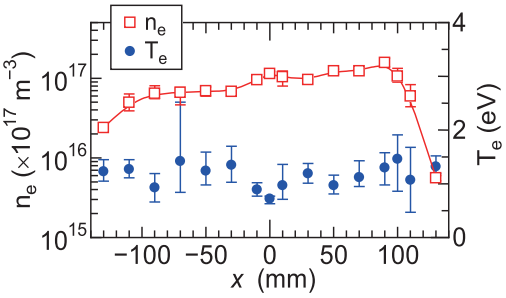

Fig. 5 Radial profiles of the electron density (open squares) and the electron temperature (filled circles) at z = 550 mm for the same condition as in Fig. 3 in configuration B.

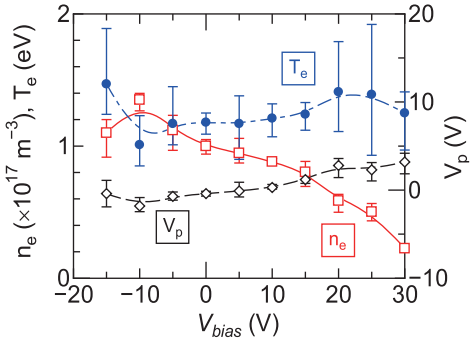

Fig. 6 The electron density (open squares), the electron temperature (filled circles), and plasma potential (open diamonds) as a function of V_{bias} measured at z = 600 mm for the same condition as in Fig. 3 in configulation B.

is voltage between the plasma grid and diffusion chamber, for magnetic filter configurations A (filled circles) and B (open squares). The electron density and the electron temperature are similar at z = 150 mm for both configurations. Figure 3 (a) shows that the higher electron density and lower electron temperature are obtained in the expansion region (z = 300 - 600 mm) for configuration B compared with those for the configuration A. The electron temperature of about 1 eV, which is required for the N-NBI operation, is obtained for configuration B, i.e., by increasing the strength of the magnetic filter. The axial transit time of the electrons is expected to increase because the axial diffusion coefficient is reduced by the factor of $1+\omega_{ce}\tau$ when applying the vertical magnetic field, where ω_{ce} is the electron cyclotron frequency and τ is the collision time. The electron energy is considered to be efficiently transferred to the neutrals via inelastic collisional processes, such as ionization and excitation for the longer transit time, which will lead the high electron density and low electron temperature. These effects are enhanced by the strength of the filter magnetic field, as observed in configuration B. Because configuration B, which has high electron density and low electron temperature, is more suitable than A for the negative ion source, all the data shown hereafter are taken in configuration B.

Figure 4 shows the electron density (open squares) and electron temperature (filled circles) measured at z = 370 mm (upstream of the magnetic filter) as a function of the gas pressure for P_{rf} = 18 kW and the matching frequency of 290 kHz. The high density hydrogen plasma having a density greater than 10^{18} m^{-3} is sustained for a pressure less than 0.3 Pa with an electron temperature of about 3 eV. The electron temperature measured near the open exit of the driver region seems to be slightly lower than that for the previous experiments using a 70-mm-diameter source ceramic tube (T_e = 4 eV) [16]. This is qualitatively understood by the particle balance analysis for the various source diameters [17].

Figure 5 shows radial distributions of the electron density and the electron temperature taken at z = 550 mm (within the magnetic filter) for the gas pressure of 0.3 Pa, P_{rf} = 18 kW, and matching frequency of 290 kHz. The low electron temperature of about 1 eV is maintained over the radial position of the measurement. The electron density is about 1×10^{17} m^{-3} at the center and is asymmetric along the x axis. The asymmetric density profile seems to be caused by the $\nabla B \times B$ drift arising from the non-uniform axial profile of the magnetic filter field, as suggested in Ref. [18]. The asymmetric density profile has to be improved hereafter and remains a further experimental issue.

In a typical rf plasma source, a positive ion sheath, which has a potential drop reflecting the electrons and negative ions, is often formed near the plasma wall boundary. The effect of the bias voltage V_{bias} is herein investigated to control the sheath structure. Figure 6 shows the electron density (open squares), the electron temperature (filled circles), and local plasma potential (open diamonds) taken at z = 600 mm as a function of the voltage V_{bias}. Over the range being tested here (V_{bias} is changed from −20 to 30 V), the electron temperature is fairly constant at 1 ± 0.3 eV, the local plasma potential are varies from −2 to 5 V, and the electron density decreases with the increase in V_{bias}. The PG potential is higher than the local plasma potential for V_{bias} > 0 V; thus, the electrons and negative ions are expected to be efficiently extracted from the plasma to

grid system. The decrease in the electron density with the increase in V_{bias} can be interpreted by an increase in the electron loss from the plasma to PG. Because the equilibrium plasma density is mainly determined by the balance between the production and loss, the increase in the electron loss yields the decrease in the plasma density in the expansion region.

Further experiments for the extraction of negative hydrogen ions using Cs are already launched. We will report these results in the future.

4. Conclusion

The high density hydrogen plasma having a density greater than 10^{18} m^{-3} was successfully produced in a 230-mm-diameter rf ion source operated with the FET-based inverter rf power supply (~ 300 kHz) at a gas pressure of 0.3 Pa. The low electron temperature of about 1 eV is obtained near the plasma grid by increasing the magnetic filter field. Although the spatial profile of the electron temperature is uniform at nearly 1 eV, the profile of the density is not uniform near the plasma grid due to electron drift. Further experiments of profile control and ion beam extraction with Cs seeding will be performed hereafter for the large rf negative ion beam source.

[1] J. Adam, Plasma Phys. Control Fusion **29**, 443 (1987).
[2] V. Erckmann and U. Gasparino, Plasma Phys. Control. Fusion **36**, 1869 (1994).
[3] R. Hemsworth *et al.*, Nucl. Fusion **49**, 045006 (2009).
[4] K.H. Berkner *et al.*, Nucl. Fusion **15**, 249 (1975).
[5] A. Kojima *et al.*, Nucl. Fusion **51**, 08, 3049 (2011).
[6] Y. Takeiri *et al.*, Rev. Sci. Instrum. **71**, 1225 (2000).
[7] M. Bacal and M. Wada, Appl. Phys. Rev. **2**, 021305 (2015).
[8] P. J. Schneider *et al.*, Phys. Rev. B **23**, 941 (1981).
[9] E. Speth and NBI-Team, Plasma Sci. Technol. **6**, 2135 (2004).
[10] A. Ando *et al.*, Phys. Plasmas **1**, 2813 (1994).
[11] A. Masiello *et al.*, Fusion Eng. Des. **86**, 860 (2011).
[12] U. Fantz *et al.*, AIP Conf. Proc. **1655**, 040001 (2015).
[13] U. Fantz *et al.*, Nucl. Fusion **49**, 125007 (2009).
[14] U. Fantz *et al.*, Plasma Phys. Control. Fusion **49**, B565 (2007).
[15] A. Ando *et al.*, Rev. Sci. Instrum. **83**, 02B122 (2012).
[16] K. Oikawa *et al.*, Rev. Sci. Instrum. **85**, 02B124 (2014).
[17] K. Takahashi *et al.*, Rev. Sci. Instrum. **85**, 02C101 (2014).
[18] M. Hanada *et al.*, Nucl. Fusion **46**, S318 (2006).